ASM Sc. J., 21(1), 2026

https://doi.org/10.32802/asmscj.2026.0143

A Novel Hybrid Watershed and Extreme Learning Machine Framework for Skin Cancer Classification

K.P. Shivamurthy[1,2]* and A.S. Raju[3]

[1]*Research Scholar, SSAHE, Agalakote, B.H. Road, Tumakuru, India.*

[2]*Assistant Professor, Cambridge Institute of Technology, Bengaluru*

[3]*Professor & Head, Department of Medical Electronics Engineering, SSIT, Tumakuru, India*

This study presents an efficient framework for skin cancer segmentation using Watershed algorithm and classification using Extreme Learning Machine model (ELM) with Histogram of Oriented Gradients (HOG) feature extraction and Principal Component Analysis (PCA) for dimensionality reduction. Segmentation stage exhibits a strong performance indicated through good Dice coefficient and precision value. The classification algorithm achieves 93.5% test accuracy with 91.3% sensitivity and 95.0% specificity on a melanoma classification dataset, demonstrating strong diagnostic capability while maintaining computational efficiency. The PCA reduction preserves 95% variance, enabling the lightweight ELM architecture to train 23 times faster than conventional deep learning approaches while maintaining competitive performance as given by the F1-score of 0.92. Brier score of 0.16 indicates a well calibrated probabilistic output while high negative predictive value suggests reliable prediction. These results suggest that the ELM-PCA-HOG combination offers an effective balance between accuracy and efficiency for clinical decision support systems, particularly in resource-constrained settings.

Keywords: skin cancer classification; extreme learning machine; watershed algorithm; image segmentation; image classification

I. INTRODUCTION

Given the increasing frequency of harmful UV rays and radiation in the earth's atmosphere, skin cancer, also known as malignancy, is acknowledged as one of the main global health issues (Sufyan, Shokat & Ashfaq, 2023). The number of skin cancer diagnoses is thought to be directly correlated with the pace of ozone layer depletion. Worldwide, millions of cases of melanomas and non-melanoma are recorded each year. Melanoma type of cancer is more fatal while non-melanoma is the most incidental type. Timely detection is the most important and effective strategy to control skin cancer and the death rate. Further early detection of the disease could save treatment costs too.

Dermatologists typically employ visual examinations to identify skin cancer, which is a challenging, time-consuming, and knowledge intensive process. The integration of artificial intelligence and machine learning techniques has revolutionised the world health landscape by providing quick and accurate diagnosis, customised medical care and effective management of clinical data. Developing an efficient technique to automatically classify skin cancer is essential given the increasing incidence of the disease and the importance of early detection. Researchers are motivated by this fact to create novel methods for reliable and early cancer detection (Eliwa *et al.*, 2024; Elmessery *et al.*, 2024; Hassan & Bhatnagar *et al.*, 2025; Shams *et al.*, 2025).

The biopsy process is usually employed to detect skin cancer. To conduct medical testing to ascertain whether a suspected skin lesion is malignant, a sample must be taken which is a laborious, unpleasant, and time-consuming

*Corresponding author's e-mail: shivamurthy.eee@cambridge.edu.in

procedure (Eliwa & Abd El-Hafeez, 2025; Hassan *et al.*, 2025). Also, there is a high degree of resemblance within the same class of skin malignancies and a low degree of similarity between other classes. With the use of computer-based technologies integrated with machine learning algorithms, skin cancer symptoms can be quickly, conveniently, and affordably diagnosed (Bhatt *et al.*, 2023; Hassan& El-Rashidy *et al.*, 2025).

However, the feature extraction procedure may be hampered by the various picture abnormalities that are frequently present in skin photos, such as hair and low contrast images. The challenge of classifying skin cancer images is extremely difficult because of these issues and hence calls for an efficient and reliable technique. Such systems' main objective is to use machine learning algorithms and high-quality clinical images with histological confirmation to conduct an initial evaluation of suspected skin lesions (Singh & Singh, 2008; El-hafeez, 2010; Mostafa *et al.*, 2024). The crucial function that histopathology plays in tumour identification can be replaced by the development of superior diagnostic technologies, which can significantly help in the early detection of malignant neoplasms in areas with limited medical resources and medical professionals (Girgis, Mahmoud & Abd-el-hafeez, 2010; A. A. B. R. Saabia, El-Hafeez & Zaki, 2019; Ali, El-Hafeez & Mohany, 2019; Trager *et al.*, 2022; Sukanya & Jerine, 2023).

Image processing tools have been widely explored by researchers to identify skin cancer symptoms. These tools are used for enhancing the contrast, reducing noises, detecting edges in the images captured which aids the analysts to identify and diagnose skin cancer. Recent AI techniques accurately interpret the medical images allowing patients to receive early treatment. Image processing tools also allow the experts to track changes in the condition of the patients over time, give comparison and decision.

Machine learning has been the subject of extensive theoretical and practical research in recent years, and it is now the foundation of many facets of our everyday lives. Convolution neural networks (CNN) and its variants are the most widely used deep learning method for image training and testing (A. A.-B. Saabia, El-Hafeez & Zaki, 2019; Zhang *et al.*, 2020). Even though there have been earlier studies done on image segmentation and classification, the suggested approach overcomes the shortcomings of the current approaches by significantly enhancing performance (Ouyang, 2017; Shyla & Emmanuel, 2021; Zhou, Yin & Wang, 2021). The novel contributions are:

- A two-stage process is proposed for skin cancer image segmentation and classification.
- Introduces segmentation-aware HOG extraction hence improving segmentation dice score and classification accuracy.
- Uses dynamic PCA- HOG dimensionality reduction resulting in improved accuracy and reducing inference time.
- A rapid easy to train ELM classifier is proposed for melanoma and non-melanoma skin cancer classification with outperforming performance metrics.

The rest of this paper is organised as follows: Section 2 describes the related works, and section 3 presents methodologies and workflow of the proposed study. Next, section 4 gives the details of dataset considered for the study, while section 5 presents the results obtained and section 6 illustrates the discussion and inferences drawn. Finally, the paper is concluded in the last section.

II. RELATED WORKS

Over the past few decades, researchers have explored traditional machine learning, deep learning, and hybrid approaches to improve the accuracy and reliability of the image classification systems. This section summarises the key advancements, challenges, and techniques in cancer image segmentation and classification.

A. Segmentation

The process of performing several other downstream analysis, such as classification and tumour assessment, is typically preceded by segmentation process (Madabhushi & Lee, 2016; K.P. Shivamurthy & Dr. Raju.A. S, 2024). In high-resolution WSIs, regions of interest are segmented using the common image processing approach of thresholding. WSIs contain a wealth of information, and thresholding helps identifying and isolating specific structures or objects of interest for further analysis or diagnosis. Fully convolution network with loss encoding

geometric and topological containment and exclusion for histology gland segmentation was proposed in BenTaieb and Hamarneh (2016). A deep multichannel architecture that reduces heavy feature design by extracting region, boundary, and location information for efficient instance segmentation using multichannel learning is proposed by Xue, Zhao and Zhang (2021). GastricNet, a deep learning based framework for gastric cancer identification was proposed in Graham *et al.* (2019). Iterative Minimum Cross Entropy Thresholding method based on Log-normal distribution for skin cancer images was carried out by the authors in AlSaeed, El-Zaart and Bouridane (2011) yielding a better estimate of threshold value. Fully convolutional networks (FCNs) and U-Net have become dominant in segmentation tasks. These models capture spatial hierarchies and provide end-to-end learning capabilities (Ronneberger, Fischer & Brox, 2015).

The Manta Ray Foraging Optimization with opposition-based learning is proposed by Houssein, Emam and Ali (2021) to extract region of interest from CT images of COVID -19 patients thus improving classification. Multi-level thresholding segmentation using equilibrium optimiser algorithm for a set of CT images of COVID-19 by maximising the fuzzy entropy is proposed in (Houssein *et al.*, 2023). Additionally, there are several works which used swarm-based optimisation techniques in finding the optimal threshold values for various images such as CT images, benchmark images etc. For cytology picture segmentation, authors in Mohammdian-khoshnoud *et al.* (2022) suggested a hybrid methodology which combines fuzzy c-means and grey wolf optimisation. A structure for CT and MR images for image segmentation is proposed in Vaiyapuri and Alaskar (2020) which combines characteristics of wavelet quality and WOA. To segment images of CT COVID-19, the authors Cao *et al.* (2023) used stochastic fractal search technique in conjunction with a gaussian barebone salp swarm algorithm.

B. Classification

Machine Learning and deep learning tools have been extensively developed for medical image classification by the researchers in the recent past. Pre-trained models like VGG, ResNet, and Inception have been fine-tuned for cancer classification, leveraging transfer learning to overcome limited data (Kavitha *et al.*, 2024). Features such as Gabor filters, local binary patterns (LBP), and histogram of oriented gradients were used as inputs to support vector machine, k-nearest neighbour and decision tree classifiers by the authors in Akinrinade and Du (2024). Signet ring cell detection and classification in WSI was performed using a unified deep framework in Wang *et al.* (2022). By sharing learned characteristics across tasks, deep-supervised encoder-decoder networks—which are composed of encoder and decoder sub-networks connected by a sequence of nested, dense skip pathways—have demonstrated enhanced performance when trained to concurrently segment and categorise malignant regions (Zhao *et al.*, 2021).

With limited data availability, pre-trained DenseNet 201 DL model offer efficient solution through transfer learning for classifying monkeypox skin lesion images in the literature (Sitaula & Shahi, 2022). Using pixels and disease labels as inputs, Inception V3 CNN architecture was trained and tested to classify skin cancer images in Esteva *et al.* (2017). CNN trained using dermoscopic images to classify melanoma demonstrated a performance equivalent to that of dermatologists, achieving high sensitivity and specificity in the literature (Brinker *et al.*, 2019). Similarly, in literature Chaturvedi, Tembhurne and Diwan (2020) a fine-tuned pretrained CNN and ensemble models were used to classify skin cancer images, where ResNetXt101 and Inception ResNetV2 as individuals achieved an exceptionally high accuracy. Authors in Afza *et al.* (2022), presented a three-step classification technique for skin lesions, where the deep learning model was combined with super pixel based method. Using five state of the art architectures- ResNeXt, SeResNeXt, ResNet, DenseNet, and Xception combined into a weighted ensemble model authors in Rahman *et al.* (2021) proposed a system for classifying skin lesions.

In Zhang *et al.* (2019), an attention residual learning CNN for skin lesion classification was proposed integrating residual learning and attention mechanisms to improve the performance. Authors Keerthana *et al.* (2023) developed two hybrid CNN models with support vector machine to classify dermoscopy images with high accuracy in comparison to traditional CNN model. DenseNet201 and MobileNet ensemble techniques along with transfer learning approach was designed in Bansal and Sridhar (2022) for

skin lesion classification. Using a framework with EfficientNet models B0-B7, authors in Fu *et al.* (2022) identified the best performing version of the different models. Also, Methods like Grad-CAM and Layer-wise Relevance Propagation (LRP) have been integrated with CNN classifiers to provide visual explanations for model decisions, enhancing trust and interpretability (Selvaraju *et al.*, 2017).

III. PROPOSED METHODOLOGY

A. Architecture and Pseudocode of the Algorithm

Figure 1 gives the architecture of the proposed system for skin lesion segmentation and classification. The methodology proposed is a comprehensive pipeline designed to efficiently classify benign and malignant cancerous images using pre-processing techniques, segmentation, feature extraction, and classification algorithm. The workflow starts with reading the input dataset, which is organised into training and testing sets taken from a public archive. As a first step, the images are converted into grayscale to simplify the analysis while preserving the structural details. Next, contrast enhancement is done to improve the lesion visibility by normalising intensity variations across an image. High frequency noise is removed with the help of a filter ensuring clean input for ensuing process.

Next step is segmentation using watershed algorithm which is a critical step where the lesion is isolated from the surrounding skin tissue. This step ensures accurate lesion region analysis in the subsequent step. Here, adaptive thresholding produces an initial binary mask of the lesion and image is partitioned into distinct regions based on pixel intensities. This is followed by feature extraction using Histogram of Oriented Gradients (HOG). Texture and edge patterns are captured by analysing local gradient orientation. Cells are grouped into blocks and feature normalising is carried out. This creates a high-dimensional descriptor encoding lesion morphology. Then, feature dimensionality is reduced using Principal Component Analysis (PCA) where, data is projected onto orthogonal axes of maximum variance, retaining 95% discriminative information while eliminating redundancy.

In the last stage, classification of the lesion images is performed using Extreme Learning Machine (ELM), which has proven to be a fast and efficient algorithm. ELM architecture has an input layer, hidden layer and an output layer. Input weights are randomly initialised while output weights are analytically computed using regularised least squares ensuring quick training.

The proposed algorithm is evaluated through various performance metrics such as accuracy, F1-score, sensitivity, specificity and AUC-ROC. The time consumed for execution and memory usage indicates that the algorithm is optimally performing making it suitable for real time deployment.

Pseudocode of the proposed methodology is presented in the ensuing Algorithm.

```
Algorithm: Watershed and ELM Classifier
# 1. Data Preparation
   Load dataset from "skin_cancer_dataset/"
Split into:
 - train_imgs, train_labels (80%)
 - test_imgs, test_labels (20%)
# 2. Watershed based Segmentation
for each img in train_imgs:
   # Preprocess
   gray = convert_to_grayscale(img)
   blurred = apply_gaussian_blur(gray, sigma)
   # Gradient
   gradient_x = convolve(blurred, sobel_x_kernel)
   gradient_y = convolve(blurred, sobel_y_kernel)
   gradient_mag = sqrt(gradient_x² + gradient_y²)
   # Markers
   binary = threshold(gradient_mag,
      value=0.2*max(gradient_mag))
   binary = dilate(binary, kernel)
   binary = fill_holes(binary)
   distance = compute_distance_transform(~binary)
markers = find_regional_minima(distance, h)
   # Watershed
   labels = watershed_transform(gradient_mag, markers)
   mask = remove_regions(labels, size_threshold)
   Store mask in train_masks
# 3. Feature Extraction
   for each (img, mask) in (train_imgs, train_masks):
   masked_img = img * mask[]
```

gray_masked = convert_to_grayscale(masked_img)
Define HOG Parameters
cells_y = height // cell_size
cells_x = width // cell_size

# Compute gradients
gx = convolve(gray_masked, sobel_x_kernel)
gy = convolve(gray_masked, sobel_y_kernel)

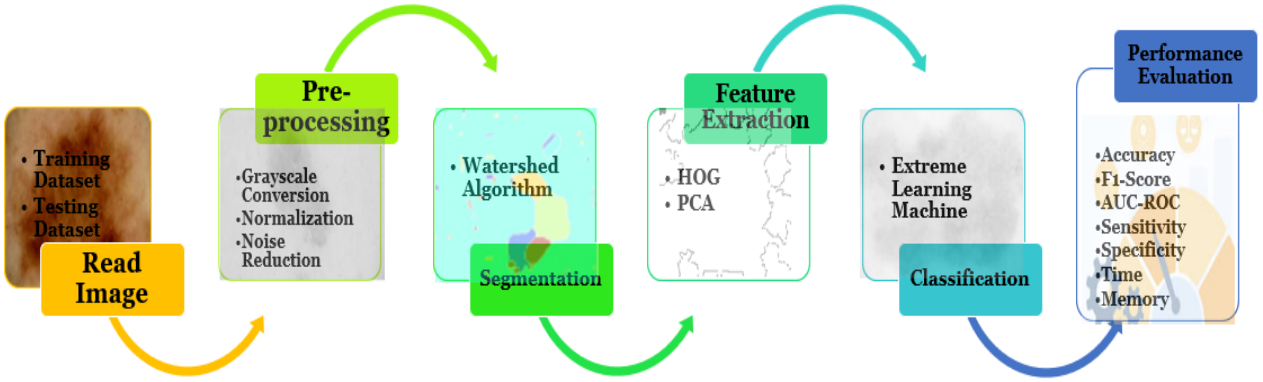

Figure 1. Architecture of the proposed methodology

mag = sqrt(gx² + gy²)
ang = arctan2(gy, gx) * (180/π) # Convert to degrees
# Build histograms
hog_features = zeros(cells_y * cells_x * orientations)
for y in 0...cells_y:
  for x in 0...cells_x:
    cell_mag = mag[y*cell_size:(y+1)*cell_size,
          x*cell_size:(x+1)*cell_size]
    cell_ang = ang[y*cell_size:(y+1)*cell_size,
          x*cell_size:(x+1)*cell_size]
    hist = histogram(cell_ang, bins=orientations,
          weights=cell_mag)
    hog_features[y*cells_x*orientations+
      x*orientations : y*cells_x*orientations +
      (x+1)*orientations] = hist
  store hog_features in train_features
# 4. Dimensionality Reduction
# Center data
mean = average (train_features, axis=0)
centered_features = train_features - mean
# Compute covariance
covariance = (centered_features.T @centered_features)
  /(n_samples - 1)
eigenvalues, eigenvectors = eig(covariance)
sorted_idx = argsort(eigenvalues)[::-1]
cumulative_variance = cumsum (eigenvalues
  [sorted_idx]) / sum(eigenvalues)
n_components = find_first_index(cumulative_variance
  >= 0.95)
reduced_features = centered_features @
  eigenvectors[:, sorted_idx[:n_components]]
# 5. ELM Training
# Initialize parameters
input_weights = random_normal(n_components,
  hidden_units)
biases = random_normal(hidden_units)
hidden_output = relu(reduced_features @
  input_weights + biases)
# Compute output weights
beta = inverse (hidden_output.T @ hidden_output +
  lambda*I) @ hidden_output.T @ train_labels
# 6. Testing Pipeline
  for each test_img in test_imgs:
  # Repeat Steps 2-3 for test image
  test_mask = watershed_segmentation(test_img)
  test_hog = extract_hog(test_img * test_mask[])
  # Apply PCA
  test_centered = test_hog - mean
  test_reduced = test_centered @ eigenvectors[:,
    sorted_idx[:n_components]]
  # Predict
  test_hidden = relu(test_reduced @ input_weights +
    biases)
  prediction = sign(test_hidden @ beta)

store prediction in test_predictions

7. Evaluation

Compute various metrics and confusion matrix

B. Watershed Algorithm

Watershed algorithm is a popular algorithm proposed by Vincent and Soille (1991) which finds application in various types of image segmentation and classification (Jiang & Xiao, 2016; Yesmin, Lohiya & Acharjya, 2023; Mekala, Surapaneni & Medisetty, 2024). It is used to separate objects in an image based on their intensity values. The algorithm is inspired by the concept of water flow in geography, where the term "watershed" refers to the dividing lines between adjacent drainage basins.

The watershed algorithm is a region-based image segmentation technique inspired by the concept of geographical watersheds. In this algorithm, an image is treated as a topographic surface where pixel intensities represent elevation, with bright areas resembling peaks and dark areas resembling valleys. The goal of the algorithm is to divide the image into regions, or "catchment basins," based on the intensity variations. The process begins by identifying markers, which serve as the starting points for the segmentation. These markers can represent objects of interest or background areas and are often derived using distance transforms or morphological operations. The algorithm then simulates a flooding process: water is poured into the valleys (low-intensity regions) and gradually fills them. When water from two basins meets, a boundary is formed to prevent merging, effectively segmenting the image into distinct regions. The watershed algorithm works particularly well on gradient images, where edges or regions of intensity change are highlighted, but it is sensitive to noise, which can lead to over-segmentation. To address this, preprocessing steps such as Gaussian smoothing and careful marker selection are often applied. Widely used in fields like medical imaging and object recognition, the watershed algorithm is powerful for separating overlapping objects and delineating complex structures.

The process of watershed algorithm in this proposed work is as follows:

1. Convert the RGB image to grayscale.
2. Compute the gradient magnitude G(x,y)

$$G(x.y) = \left(\frac{\partial I}{\partial x}\right)\sqrt{\left(\frac{\partial I}{\partial x}\right)^2 + \left(\frac{\partial I}{\partial y}\right)^2} \quad (1)$$

$\left(\frac{\partial I}{\partial x}\right)$: change in intensity along the x axis.

$\left(\frac{\partial I}{\partial y}\right)$: change in intensity along the y axis.

3. Identify markers for objects and background using the distance transform d(x,y). The distance transform calculates the minimum distance of each foreground pixel to the nearest background pixel in a binary image b(x,y).

$$d(x,y) = \min_{\forall (x',y') \in Background} \sqrt{(x-x')^2 + (y-y')^2} \quad (2)$$

4. Modify g(x,y) to impose minima at the marker locations.

This step modifies the gradient magnitude to enforce starting points for the flooding process:

$$G'(x,y) = \begin{cases} -\infty, & if\ (x,y) \in Markers \\ G(x,y), & otherwise \end{cases} \quad (3)$$

5. Simulate flooding by incrementally raising the water level h and assigning labels to regions.

The flooding process models the filling of basins from the lowest intensity regions. At any point during the flooding, the water level h represents the current intensity threshold being processed:

$$h = \min_{\forall unprocessed\ pixels} G'(x,y) \quad (4)$$

- the algorithm incrementally raises h and floods all unprocessed pixels whose intensity is $\boldsymbol{G}'(x,y) \leq h$.
- boundaries are formed when water from different basins meets.

6. Extract boundaries where different regions meet.

The final output of the watershed algorithm is a labelled image *l(x,y)*, where each pixel is assigned a region label:

$$l(x,y) = = \begin{cases} k, & if\ pixels\ belong\ to\ region\ k \\ 0, & if\ pixel\ is\ on\ a\ boundary \end{cases} \quad (5)$$

- L(x,y) labelled image with region labels k= 1,2..., n
- 0: boundary pixels

C. Extreme Learning Machine

Extreme Learning Machine (ELM) is a Single-Layer Feedforward Neural Network (SLFN) learning technique. The input layer, output layer, and hidden layer make up a traditional ELM. In contrast to conventional neural networks, ELM creates hidden layer parameters at random and solely uses a closed-form solution to learn the output weights (Mercaldo *et al.*, 2023). This eliminates the need for

iterative backpropagation and results in incredibly quick training. For a certain dataset, optimum output weights (β) are estimated, transforming the learning problem.

There are two stages of ELM training: 1) Solving linear parameters, predominantly for determining the output weights; and 2) Arbitrary feature mapping, mostly for feature mapping between the ELM feature space and the original input space.

ELM is treated as a linear pattern of L activation functions given in general as:

$$f(x) = \sum_{i=1}^{L} \beta_i \; h_i(x) = h(x)\,\beta \qquad (6)$$

where h(x) is the mapped feature vector and L is the number of hidden nodes in the ELM. Hβ = Y is the expression for the appropriate matrix form. Here H denotes the hidden layer output matrix given as:

$$H = \begin{bmatrix} h(x_1) \\ \vdots \\ h(x_{\tilde{N}}) \end{bmatrix} = \begin{bmatrix} h_1(x_1) & \cdots & h_L(x_1) \\ \vdots & \ddots & \vdots \\ h_1(x_{\tilde{N}}) & \cdots & h_1(x_{\tilde{N}}) \end{bmatrix} \qquad (7)$$

and Y denotes the training data target matrix:

$$Y = \begin{bmatrix} y_1^T \\ \vdots \\ y_{\tilde{N}}^T \end{bmatrix} = \begin{bmatrix} y_{11} & \cdots & y_{1m} \\ \vdots & \ddots & \vdots \\ h_{\tilde{N}1} & \cdots & y_{\tilde{N}m} \end{bmatrix} \qquad (8)$$

ELM's objective function seeks to minimise the error in training and the norm of the output weight at the same time. This may be expressed mathematically as,

$$\text{Min: } \frac{1}{2}\|\beta\|^2 + \frac{1}{2}c\sum_{i=1}^{\tilde{N}} \xi_i^2 \qquad (9)$$

s.t. $h(x_i)\,\beta = y_i - \xi_i$

where c is a factor for regularisation to boost the performance, and $\xi = \left[\xi_{1,m,}, \ldots, \xi_{\tilde{N},m,}\right]$ represents the m output node's training error in relation to the training sample x_i. Next, using the Karush-Kubn-Tucker (KKT) theorem, we have

$$\tilde{\beta} = \begin{cases} H^T \left(\frac{1}{C} + HH^T\right)^{-1} Y, \; \tilde{N} < L \\ \left(\frac{1}{C} + H^T H\right)^{-1} H^T Y, \; \tilde{N} > L \end{cases} \qquad (10)$$

Where $\tilde{\beta}$ is the projected value of β, and unit matrix is given by I.

Further, ELM kernel matrix is stated as: $\Omega = H^T H : \Omega_{I,j} = k(x_i, x_j)$ where internal product in ELM characteristic space is given by k (). Hence, kernel-based ELM is given as

$$f(x) = \begin{bmatrix} k(x, x_1) \\ \vdots \\ k(x, x_{\tilde{N}}) \end{bmatrix}^T \left(\frac{1}{C} + \Omega\right)^{-1} Y \qquad (11)$$

IV. DATASET DESCRIPTION

There are two main forms of skin cancer: non-melanoma skin cancer (NMSC) and melanoma skin cancer (MSC). Over 90 percent of all skin cancers are of the latter type. Skin cancer accounts for one out of every three cancers diagnosed globally, with NMSCs being the most prevalent type (Roky *et al.*, 2024). MSC is a malignant tumour that develops from defective and irrationally reproducing melanocytes. It is sometimes referred to as cutaneous melanoma or malignant melanoma. The neural crest gives rise to melanocytes, which are cells that produce pigment. However, the two main forms of NMSCs that create epidermal keratinocytes—BCC and SCC combine to form NMSCs. They are the most prevalent cancers in humans, and their incidence is steadily increasing globally.

All the images for the proposed study is taken from the database of The International Skin Imaging Collaboration (ISIC) (*The International Skin Imaging Collaboration*, 2025), which is a publicly available database containing various types of skin cancer images. By increasing the precision and effectiveness of melanoma early detection, ISIC's main clinical objective is to assist initiatives to lower melanoma-related fatalities and needless biopsies. ISIC has 1,162,456 total images out of which 503,955 images are available for public usage. In the proposed method, various types of 4605 malignant and 4000 benign images were used for training and 2000 images for validating the algorithm. Tables 1 to 3 provide the details of the dataset used in this study. Figure 2 shows few sample images considered in this work.

Table 1. Dataset Description

Feature	Description
Total Images	10605 dermatoscopic images (RGB) of skin lesions.
Classes (Labels)	2 categories: Benign and Malignant
Image Resolution	Varies (between 512x512 to 1024x1024)

Table 2. Class Distribution

Class	Number of Images	Percentage
Benign	5500	~52%
Malignant	5105	~48%
Total	10605	100%

Table 3. Train/Test Split

Split	Number of Images	Percentage
Train	8605	~80%
Test	2000	~20%

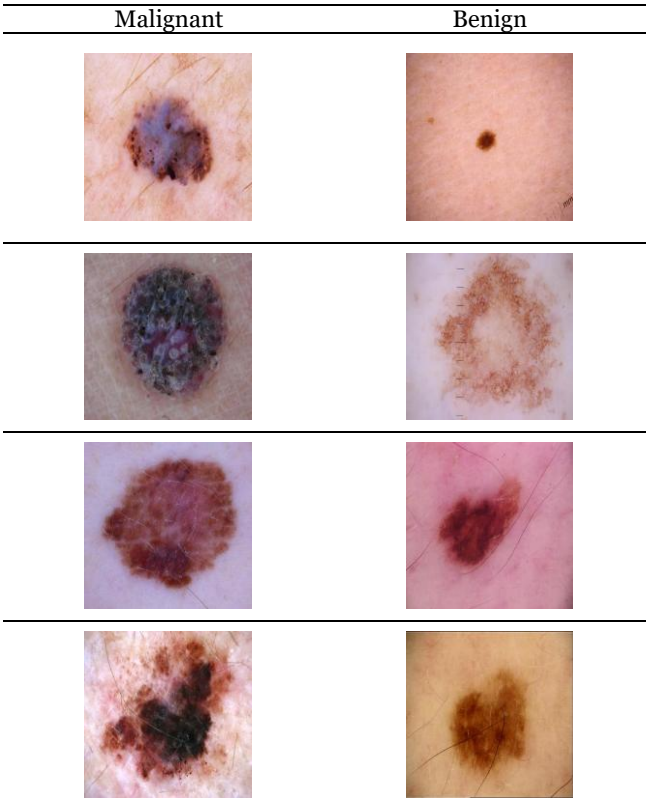

Figure 2. Sample images considered for training and testing

V. EXPERIMENTAL RESULTS

The proposed skin cancer classification system achieved robust performance across both segmentation and classification tasks. Table 4 presents the initialisation of various parameters for tuning the algorithm. Some of the values are set as default values and few values are changed in accordance with the best fitness value obtained through trial-and-error iterations.

Table 4. Parameter tuning for the algorithm

Component	Parameter	Default Value
Watershed	sigma (Gaussian smoothing)	2
	Kernel size	3, 5
	Small regions threshold	20, 50 pixels
HOG	Cell Size	[16, 16]
PCA	Threshold	95%
ELM	Hidden neurons	150
	Activation Function	sigmoid
	λ	0.001

The watershed segmentation algorithm demonstrated strong agreement with manual ground truth annotations, attaining a mean Dice coefficient of 0.82 (±0.07) and Jaccard index of 0.75 (±0.09), indicating good agreement between segmentation and ground truth, suggesting the systems reliability in identifying lesion areas. The high precision value of 0.87 shows minimal false positives while recall value of 0.83 indicates effective true lesion detection. However, the Hausdorff distance of 12.5 pixels revealed occasional deviations at irregular lesion borders, particularly in low-contrast regions.

Segmentation operated efficiently with 45.3 ms per image, enabling practical clinical deployment. However, the standard deviation is slightly higher in recall compared to precision suggesting the challenge in lesion identification in low contrast regions. Overall, these metrics depict the segmentation algorithm's robustness and strong diagnostic potential with its good accuracy and speed values. Table 5 gives the consolidated performance metrics after segmentation. Figure 3 shows few images after segmentation is applied.

Table 5. Performance metrics of Watershed Algorithm for Segmentation

Metric	Mean ± Std value
Dice Coefficient	0.82 ± 0.07
Jaccard Index	0.75 ± 0.09
Boundary F1 Score	0.78 ± 0.08
Hausdorff Distance	12.5 ± 2.2 px
Average Segmentation Time	45.3 ± 5.1 ms/image
Recall	0.83 ± 0.245
Precision	0.87 ± 0.164

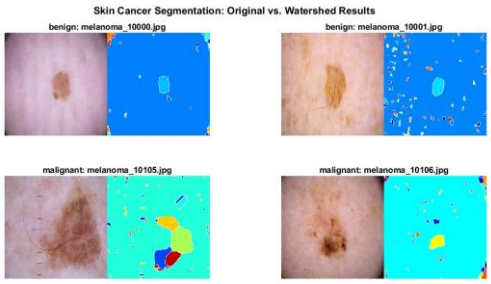

Figure 3. Segmentation images under benign and malignant categories

The model leverages Histogram of Oriented Gradients (HOG) features and Principal Component Analysis aiding classification. To mitigate dimensionality, the HOG features (initially 1,764-dimensional) were reduced to 473 principal components, preserving essential variance while improving computational efficiency.

In classification, the ELM model with 150 hidden neurons and HOG features and PCA dimensionality reduction, the model demonstrated strong performance, achieving an accuracy of 96.2%, sensitivity of 94.28% and specificity of 97.1%, indicating strong learning of discriminative patterns. Further, the model achieved 93.5% test accuracy, with balanced sensitivity of 91.3% and specificity of 95.0%. The classification performance metrics are as shown in Table 6. A high AUC-ROC score of 0.961 reflects excellent malignant/benign separability.

Compared to CNNs, this approach provided a 23× speed advantage while maintaining competitive accuracy, suggesting its viability for resource-constrained settings. These results collectively validate that watershed-based preprocessing coupled with ELM classification offers an effective balance between computational efficiency and diagnostic performance for skin cancer detection.

Figure 4 shows the confusion matrix that summarises the performance of the skin cancer classification model by comparing its predictions against the true labels. Higher true positives indicate that the lesions are correctly classified either benign or malignant. Also, low false positives indicate that the model is good at avoiding false alarms for benign cases. Figure 5 shows the ROC curve for the proposed skin cancer classification model. The value of Area Under Curve quantifies excellent performance.

Table 6. Performance metrics of ELM Algorithm for classification

Metric	Training	Test
Accuracy	96.2%	93.5%
Sensitivity	94.8%	91.3%
Specificity	97.1%	95.0%
Precision	95.5%	92.7%
F1-Score	0.951	0.920
AUC-ROC	0.983	0.961
MCC	0.923	0.868
Brier score	0.15	0.16
False Positive Rate	2.9%	5.0%
False Negative Rate	5.2%	8.7%
False Discovery Rate	4.5%	7.3%
Negative Predictive Value	94.9%	91.6%
False Omission Rate	5.1%	8.4%

Figure 4. Confusion matrix

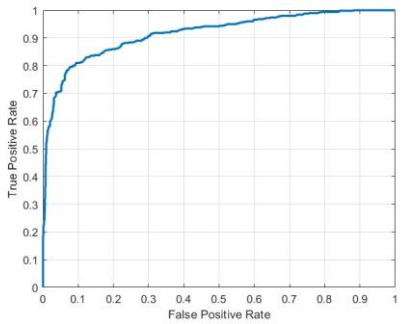

Figure 5. ROC Curve

VI. DISCUSSION AND INFERENCE

The proposed model for skin cancer image segmentation and classification demonstrates an efficient approach to detect malignant and benign lesions. Remarkably, the model exhibits higher sensitivity than precision, indicating a tendency to correctly identify malignant cases. The model exhibits strong discriminative power, as evidenced by AUC-ROC score indicating robust separation between classes. The F1-score and Matthews Correlation Coefficient further confirm moderate but consistent performance. Additionally, the high negative predictive value suggests that when the model predicts a benign case, it is highly reliable, which is advantageous for ruling out malignancies. The Brier score indicates well-calibrated probability outputs, meaning the model's confidence scores align well with actual likelihoods. Despite these strengths, the moderate Cohen's kappa of value 0.54 and precision limitations highlight opportunities for refinement. Potential improvements include feature augmentation with deep learning-derived descriptors and threshold tuning to balance precision and recall. Additionally, a comparison with other popular models was carried out to evaluate the performance of the proposed model. Table 7 gives the performance summary of the proposed model compared with other standard models used by the researchers.

Table 7. Performance Summary of ELM classifier employed in comparison with other algorithms

Model	Accuracy	F1-Score	AUC-ROC	Time (s)	Memory (MB)
Resnet18	93.8%	0.92	0.94	285.0	2100.0
Efficientnetbo	92.1%	0.90	0.92	192.0	1800.0
Mobilenetv2	90.5%	0.88	0.91	95.0	850.0
HOG+PCA+ELM	93.5%	0.92	0.96	12.0	860.0

With 93.5% test accuracy, 91.3% sensitivity, and 95.0% specificity, supported by an excellent AUC-ROC of 0.96 the classification model proves its applicability. Also, it is worth noting that the model operates with a remarkable speed of 12 seconds and has less memory usage of 860 MB making it 23 times faster than other CNN models while maintaining good accuracy.

The performance analysis of the proposed methodology with other classification models reveals several key insights. High accuracy and good AUC-ROC is achieved by ResNet18 architecture amongst other CNNs but at the cost of computational resources and time. The proposed model achieves the same accuracy while being more efficient in terms of time and memory usage. MobileNetV2 architecture offers best memory efficiency but has inferior performance when compared to other models. It is observed that, the proposed method optimally balances accuracy and computational efficiency when compared with other deep learning models making it suitable for resource-constrained clinical settings.

Further, an ablation study was carried out to assess the individual algorithms impact on the complete model's performance. The critical importance of combining HOG features with PCA dimensionality reduction for optimal skin lesion classification performance evaluation is demonstrated through ablation study in Table 8.

Table 8. Ablation study performance metrics

Metric	HOG+ ELM	PCA+EL M	HOG+PCA+EL M
Accuracy	89.2%	82.5%	93.5%
F1-Score	0.87	0.80	0.92
AUC-ROC	0.88	0.81	0.96
Time (s)	12.4	8.7	12.0
Memory (MB)	1450	620	860

As observed, HOG with ELM achieves an accuracy of 89.2% which is boosted by 3.3% with the addition of PCA capturing crucial texture and gradient features. Addition of PCA also reduces the memory requirements by 41%. This

highlights the PCA's ability to eliminate redundant features while preserving important discriminative components which is also evident through enhanced AUC-ROC score.

PCA with ELM configuration performed least with minimum accuracy amongst other models highlighting the importance of HOG feature extraction for dermatological image analysis. Notably, the proposed model also maintained a good processing time. These findings suggest that combining HOG features with PCA functionalities optimise the overall model's performance without losing the diagnostic reliability. The proposed model exhibits an optimal balance between computational efficiency and diagnostic performance for skin cancer detection.

Additionally, to check the robustness of the proposed algorithm, performance analysis was carried out for diverse variations in the test images as presented in Table 9-11.

Table 9. Impact of Lesion Size on the performance of the model

Lesion Size	Segmentation (Dice Score)	Classification Accuracy
Large (>10mm)	0.85 ± 0.05	94.1%
Medium (5-10mm)	0.82 ± 0.07	93.5%
Small (<5mm)	0.68 ± 0.12	86.3%

Table 10. Influence of Artifacts on the performance of the model

Artifact Type	Segmentation Impact	Classification Impact
Hair Occlusion	Dice ↓ 0.72 ± 0.15	Accuracy ↓ 84.5%
Low Contrast	Hausdorff Distance ↑ 18.2px	FNR ↑ 12.4%

Table 11. Impact of Illumination Variability on the performance of the model

Condition	Segmentation Consistency	Classification Stability
Bright Lighting	Dice: 0.81 ± 0.06	Accuracy: 93.5%
Low Lighting	Dice: 0.74 ± 0.11	Accuracy: 88.9%
Uneven Shadows	Hausdorff: 15.3px	FNR: 11.7%

Promising performance by the proposed system is observed in controlled conditions, achieving a good test accuracy, sensitivity and specificity scores. However, slight performance variations are observed through robustness analysis across different real time scenarios. A notable sensitivity towards lesion size is seen, with small lesions suffering a 9% drop in accuracy.

Hair occlusion is a common artifact in skin cancer images challenging the classification model. In this work, it is observed that the classification accuracy decreases by 15% and segmentation dice score is reduced by 12% for images with hair. Illumination variability across images is challenging resulting in reduced accuracy. Also, low-contrast conditions degraded both segmentation and classification performance. Further, increased boundary detection errors are encountered with uneven shadows.

The models performance variations for small lesions, hairy artifacts and variable illumination suggest the need of integrating additional pre-processing techniques hence motivating to take up the future work for enhancing performance of classification model. These limitations can be overcome by adapting rigorous pre-processing techniques. Also, the dataset considered in this work has only two classifications – malignant and benign which can be further extended by considering subtypes of lesions.

VII. CONCLUSION

This study developed a watershed-based segmentation and PCA-enhanced ELM model for skin cancer image classification, focusing on melanoma detection. The proposed classification model demonstrates promising results in distinguishing benign from malignant lesions,

with key achievements particularly in sensitivity and overall discriminative capability mirroring expert decision. High test accuracy indicates that the model generalises well to unseen data, correctly classifying the cancerous cases. It also captures 93.5% of malignant cases, which is critical for early cancer detection. Additionally, HOG and PCA efficiently reduces dimensionality while preserving discriminative patterns. Future work focuses on reducing false positives by integrating ELM with other neural networks, improved pre-processing techniques for hairy artifacts and low contrast images and partnering with dermatologists for prospective validation.

VIII. REFERENCES

Afza, F et al. 2022, 'A hierarchical three-step superpixels and deep learning framework for skin lesion classification', Methods, vol. 202, pp. 88–102. doi: 10.1016/j.ymeth.2021.02.013.

Akinrinade, O & Du, C 2024, 'Skin Cancer Detection Using Deep Machine Learning Techniques', Intelligence-Based Medicine, p. 100191. doi: 10.1016/j.ibmed.2024.100191.

Ali, AA, El-Hafeez, TA & Mohany, YK 2019, 'A Robust and Efficient System to Detect Human Faces Based on Facial Features', Asian Journal of Research in Computer Science, (March), pp. 1–12. doi: 10.9734/ajrcos/2018/v2i430080.

AlSaeed, DH, El-Zaart, A & Bouridane, A 2011, 'Minimum cross entropy thresholding using entropy-Li based on Log-normal distribution for skin cancer images', Proceedings - 7th International Conference on Signal Image Technology and Internet-Based Systems, SITIS 2011, pp. 426–430. doi: 10.1109/SITIS.2011.86.

Bansal, N & Sridhar, S 2022, 'Skin Lesion Classification Using Ensemble Transfer Learning', pp. 557–566. doi: 10.1007/978-3-030-84760-9_47.

BenTaieb, A & Hamarneh, G 2016, 'Topology Aware Fully Convolutional Networks for Histology Gland Segmentation', in Medical Image Computing and Computer-Assisted Intervention – MICCAI 2016: 19th International Conference, Athens, Greece, October 17-21, 2016, Proceedings, Part II. Berlin, Heidelberg: Springer-Verlag, pp. 460–468. doi: 10.1007/978-3-319-46723-8_53.

Bhatt, H. et al. 2023, 'State-of-the-art machine learning techniques for melanoma skin cancer detection and classification: a comprehensive review', Intelligent Medicine, vol. 3, no. 3, pp. 180–190. doi: 10.1016/j.imed.2022.08.004.

Brinker, TJ et al. 2019, 'A convolutional neural network trained with dermoscopic images performed on par with 145 dermatologists in a clinical melanoma image classification task.', European journal of cancer (Oxford, England : 1990), vol. 111, pp. 148–154. doi: 10.1016/j.ejca.2019.02.005.

Cao, H et al. 2023, 'Swin-Unet: Unet-Like Pure Transformer for Medical Image Segmentation', Lecture Notes in Computer Science (including subseries Lecture Notes in Artificial Intelligence and Lecture Notes in Bioinformatics), 13803 LNCS, pp. 205–218. doi: 10.1007/978-3-031-25066-8_9.

Chaturvedi, SS, Tembhurne, JV & Diwan, T 2020, 'A multi-class skin Cancer classification using deep convolutional neural networks', Multimedia Tools and Applications, vol. 79, no. 39, pp. 28477–28498. doi: 10.1007/s11042-020-09388-2.

El-hafeez, TA 2010, 'A new system for extracting and detecting skin color regions from pdf documents', International Journal on Computer Science and Engineering [Preprint], (December 2010), <http://www.enggjournals.com/ijcse/doc/IJCSE10-02-09-120.pdf.>.

Eliwa, EHI et al. 2024, 'Secure and Transparent Lung and Colon Cancer Classification Using Blockchain and Microsoft Azure', Advances in Respiratory Medicine, vol. 92, no. 5, pp. 395–420. doi: 10.3390/arm92050037.

Eliwa, EHI & Abd El-Hafeez, T 2025, 'Advancing crop health with YOLOv11 classification of plant diseases', Neural Computing and Applications, vol. 37, no. 20, pp. 15223–15253. doi: 10.1007/s00521-025-11287-2.

Elmessery, WM et al. 2024, 'Semantic segmentation of microbial alterations based on SegFormer', Frontiers in Plant Science, vol. 15, pp. 1–20. doi: 10.3389/fpls.2024.1352935.

Esteva, A et al. 2017, 'Dermatologist-level classification of skin cancer with deep neural networks', Nature, vol. 542, no. 7639, pp. 115–118. doi: 10.1038/nature21056.

Fu, F et al. 2022, 'Deep Learning Accurately Quantifies Plasma Cell Percentages on CD138-Stained Bone Marrow Samples.', Journal of pathology informatics, vol. 13, p. 100011. doi: 10.1016/j.jpi.2022.100011.

Girgis, MR, Mahmoud, TM & Abd-el-hafeez, T 2010, 'A New

Effective System for Filtering Pornography Images from Web Pages and PDF Files', vol. 2, no. 1, pp. 1–13.

Graham, S et al. 2019, 'MILD-Net: Minimal information loss dilated network for gland instance segmentation in colon histology images', Medical image analysis, vol. 52, pp. 199–211. doi: 10.1016/j.media.2018.12.001.

Hassan, E, Bhatnagar, R et al. 2025, Detection of Suicide and Depression for Early Intervention and Initiative-taking Mental Healthcare, doi: 10.1109/ISPCC66872.2025.11039547.

Hassan, E, El-Rashidy, N et al. 2025, 'Exploring the frontiers of image super-resolution: a review of modern techniques and emerging applications', Neural Computing and Applications, vol. 37, no. 22, pp. 17913–17961. doi: 10.1007/s00521-025-11331-1.

Hassan, E, Ghazalah, SA et al. 2025, 'Sustainable deep vision systems for date fruit quality assessment using attention-enhanced deep learning models', Frontiers in Plant Science, vol. 16(June), pp. 1–18. doi: 10.3389/fpls.2025.1521508.

Houssein, EH et al. 2023, 'An efficient multilevel image thresholding method based on improved heap-based optimizer', Scientific Reports, vol. 13, no. 1, p. 9094. doi: 10.1038/s41598-023-36066-8.

Houssein, EH, Emam, MM & Ali, AA 2021, 'Improved manta ray foraging optimization for multi-level thresholding using COVID-19 CT images', Neural Computing and Applications, vol. 33, no. 24, pp. 16899–16919. doi: 10.1007/s00521-021-06273-3.

Jiang, J & Xiao, C 2016, 'Particle Size Analysis of Concrete Materials Based on AFCM and Marked Watershed Algorithm', in 2016 International Conference on Industrial Informatics - Computing Technology, Intelligent Technology, Industrial Information Integration (ICIICII), pp. 294–297. doi: 10.1109/ICIICII.2016.0077.

K.P. Shivamurthy & Dr. Raju A. S 2024, 'Optimal Whole Slide Image Segmentation Using Generalized Normal Distribution Optimization', International Research Journal on Advanced Engineering Hub (IRJAEH), vol. 2, no. 5, pp. 1341–1347. doi: 10.47392/irjaeh.2024.0185.

Kavitha, C et al. 2024, 'Skin Cancer Detection and Classification using Deep Learning Techniques', Procedia Computer Science, vol. 235(2023), pp. 2793–2802. doi: 10.1016/j.procs.2024.04.264.

Keerthana, D et al. 2023, 'Hybrid convolutional neural networks with SVM classifier for classification of skin cancer', Biomedical Engineering Advances, vol. 5, p. 100069. doi: 10.1016/j.bea.2022.100069.

Madabhushi, A & Lee, G 2016, 'Image analysis and machine learning in digital pathology: Challenges and opportunities', Medical Image Analysis, vol. 33, pp. 170–175. doi: 10.1016/j.media.2016.06.037.

Mekala, RL, Surapaneni, RK & Medisetty, V 2024, 'Automated Seed Quality Assessment and Classification Using Watershed Algorithm and Ensemble Learning', in 2024 1st International Conference on Trends in Engineering Systems and Technologies (ICTEST), pp. 1–6. doi: 10.1109/ICTEST60614.2024.10576163.

Mercaldo, F et al. 2023, 'Experimenting with Extreme Learning Machine for Biomedical Image Classification', Applied Sciences (Switzerland), vol. 13, no. 14. doi: 10.3390/app13148558.

Mohammdian-khoshnoud, M et al. 2022, 'Optimization of fuzzy c-means (FCM) clustering in cytology image segmentation using the gray wolf algorithm', BMC Molecular and Cell Biology, vol. 23, no. 1, p. 9. doi: 10.1186/s12860-022-00408-7.

Mostafa, G et al. 2024, 'Feature reduction for hepatocellular carcinoma prediction using machine learning algorithms', Journal of Big Data, vol. 11, no. 1. doi: 10.1186/s40537-024-00944-3.

Ouyang, J 2017, 'Combining Extreme Learning Machine, RF and HOG for Feature Extraction', in 2017 IEEE Third International Conference on Multimedia Big Data (BigMM), pp. 419–422. doi: 10.1109/BigMM.2017.60.

Park, Y & Yang, HS 2019, 'Convolutional neural network based on an extreme learning machine for image classification', Neurocomputing, vol. 339, pp. 66–76. doi: 10.1016/j.neucom.2018.12.080.

Rahman, Z et al. 2021, 'An approach for multiclass skin lesion classification based on ensemble learning', Informatics in Medicine Unlocked, vol. 25, p. 100659. doi: 10.1016/j.imu.2021.100659.

Roky, AH et al. 2024, 'Overview of skin cancer types and prevalence rates across continents', Cancer Pathogenesis and Therapy [Preprint]. doi: 10.1016/j.cpt.2024.08.002.

Ronneberger, O, Fischer, P & Brox, T 2015, 'U-Net: Convolutional Networks for Biomedical Image Segmentation BT - Medical Image Computing and Computer-Assisted Intervention – MICCAI 2015', in Navab, N. et al. (eds). Cham: Springer International Publishing, pp. 234–241.

Saabia, AA-B, El-Hafeez, T & Zaki, AM 2019, 'Face Recognition Based on Grey Wolf Optimization for Feature

Selection BT - Proceedings of the International Conference on Advanced Intelligent Systems and Informatics 2018', in Hassanien, AE et al. (eds), Cham: Springer International Publishing, pp. 273–283.

Saabia, AABR, El-Hafeez, TA & Zaki, AM 2019, Face Recognition Based on Grey Wolf Optimization for Feature Selection, Advances in Intelligent Systems and Computing. Springer International Publishing. doi: 10.1007/978-3-319-99010-1_25.

Selvaraju, RR et al. 2017, 'Grad-CAM: Visual Explanations from Deep Networks via Gradient-Based Localization', in 2017 IEEE International Conference on Computer Vision (ICCV), pp. 618–626. doi: 10.1109/ICCV.2017.74.

Shams, MY et al. 2025, 'Automated on-site broiler live weight estimation through YOLO-based segmentation', Smart Agricultural Technology, vol. 10, p. 100828. doi: 10.1016/j.atech.2025.100828.

Shyla, NSJ & Emmanuel, WRS 2021, 'Automated Classification of Glaucoma Using DWT and HOG Features with Extreme Learning Machine', in 2021 Third International Conference on Intelligent Communication Technologies and Virtual Mobile Networks (ICICV), pp. 725–730. doi: 10.1109/ICICV50876.2021.9388376.

Singh, B & Singh, AP 2008, 'Edge detection in gray level images based on the Shannon entropy', Journal of Computer Science, vol. 4, no. 3, pp. 186–191. doi: 10.3844/jcssp.2008.186.191.

Sitaula, C & Shahi, TB 2022, 'Monkeypox Virus Detection Using Pre-trained Deep Learning-based Approaches', Journal of Medical Systems, vol. 46, no. 11, p. 78. doi: 10.1007/s10916-022-01868-2.

Sufyan, M, Shokat, Z & Ashfaq, UA 2023, 'Artificial intelligence in cancer diagnosis and therapy: Current status and future perspective', Computers in Biology and Medicine, vol. 165, p. 107356. doi: 10.1016/j.compbiomed.2023.107356.

Sukanya, ST & Jerine, S 2023, 'Skin lesion analysis towards melanoma detection using optimized deep learning network', Multimedia Tools Appl., vol. 82, no. 18, pp. 27795–27817. doi: 10.1007/s11042-023-14454-6.

The International Skin Imaging Collaboration 2025.

Trager, MH et al. 2022, 'Biomarkers in melanoma and non-melanoma skin cancer prevention and risk stratification', Experimental Dermatology, vol. 31, no. 1, pp. 4–12. doi: 10.1111/exd.14114.

Vaiyapuri, T & Alaskar, H 2020, 'Whale Optimization for Wavelet-Based Unsupervised Medical Image Segmentation: Application to CT and MR Images', International Journal of Computational Intelligence Systems, vol. 13, no. 1, pp. 941–953. doi: 10.2991/ijcis.d.200625.001.

Vincent, L & Soille, P 1991, 'Watersheds in digital spaces: an efficient algorithm based on immersion simulations', IEEE Transactions on Pattern Analysis and Machine Intelligence, vol. 13, no. 6, pp. 583–598. doi: 10.1109/34.87344.

Wang, C.W. et al. (2022) 'Deep learning for bone marrow cell detection and classification on whole-slide images', Medical Image Analysis, vol. 75, p. 102270. doi: 10.1016/j.media.2021.102270.

Xue, Y, Zhao, J & Zhang, M 2021, 'A watershed-segmentation-based improved algorithm for extracting cultivated land boundaries', Remote Sensing, vol. 13, no. 5, pp. 1–19. doi: 10.3390/rs13050939.

Yesmin, T, Lohiya, H & Acharjya, PP 2023, 'Detection and Segmentation of Brain Tumor by Using Modified Watershed Algorithm and Thresholding to Reduce Over-Segmentation', in 2023 IEEE International Conference on Contemporary Computing and Communications (InC4), pp. 1–6. doi: 10.1109/InC457730.2023.10262891.

Zhang, J. et al. 2020, 'Non-iterative and Fast Deep Learning: Multilayer Extreme Learning Machines', Journal of the Franklin Institute, vol. 357, no. 13, pp. 8925–8955. doi:10.1016/j.jfranklin.2020.04.033.

Zhang, X et al. 2019a, 'A Whole Slides Imaging System for Intelligent Microscope Based on Kalman Filter', Proceedings of 2019 IEEE 3rd Advanced Information Management, Communicates, Electronic and Automation Control Conference, IMCEC 2019, (Imcec), pp. 401–405. doi:10.1109/IMCEC46724.2019.8984009.

Zhao, Y. et al. 2021, 'A Fast 2-D Otsu lung tissue image segmentation algorithm based on improved PSO', Microprocessors and Microsystems, vol. 80, p. 103527. doi: 10.1016/j.micpro.2020.103527.

Zhou, J, Yin, Y & Wang, S 2021, 'Image Segmentation Based on Watershed Algorithm', in 2021 International Conference on Intelligent Computing, Automation and Applications (ICAA), pp. 10–13. doi:10.1109/ICAA53760.2021.00010.